Optimal Control of Shunt Active Power Filter to Meet IEEE Std. 519 Current Harmonic Constraints Under Nonideal Supply Condition

Parag Kanjiya, Vinod Khadkikar, *Member, IEEE*, and Hatem H. Zeineldin, *Senior Member, IEEE*

***Abstract*—A shunt active power filter (APF) is a well-mature technology for the compensation of nonlinear and/or reactive loads. Normally, the shunt APF is controlled such that it eliminates the load current harmonics and supplies load reactive power to achieve harmonic-free source currents at unity power factor. However, these control objectives cannot be achieved simultaneously when the supply voltages are distorted and unbalanced (nonideal). Hence, under such situation, the shunt APF should be controlled optimally to achieve a maximum possible power factor without violating the current harmonic constraints recommended by IEEE Std. 519. This paper presents an optimal algorithm to control a three-phase four-wire shunt APF under nonideal supply conditions. The optimization problem aiming at maximizing the power factor subject to current harmonic constraints as per IEEE Std. 519 has been formulated and solved mathematically using the Lagrangian formulation. The proposed algorithm avoids the use of complex iterative optimization techniques and thus is simple to implement and has fast dynamic response. The effectiveness of the proposed method is evaluated through a detailed experimental investigation using a digital signal processor controlled shunt APF prototype developed in the laboratory.**

***Index Terms*—Active power filter (APF), harmonic compensation, optimized control, power quality, unity power factor (UPF).**

I. Introduction

THE electrical power distribution system is one of the most vulnerable systems to power quality problems, such as increased voltage/current distortion levels due to the widespread use of power-electronics-based nonlinear loads. Furthermore, the three-phase four-wire (3P4W) distribution system possesses the problem of excessive neutral current and current unbalance due to the uneven distribution of single-phase loads. This has resulted in increased voltage and current harmonics, unbalance in supply voltages and currents, excessive neutral current, poor power factor, increased losses, and reduced overall efficiency.

The shunt active power filter (APF) is a well-proven technology to suppress most of the load-current-originated power quality problems in both three-phase three-wire and 3P4W systems [1]. The work related to different shunt APF control strategies for the load compensation is well documented in [2]–[14]. The most widely adopted APF control strategies for the load compensation can be identified as follows: 1) harmonic-free (HF) source currents and 2) unity power factor (UPF) source currents. Both strategies lead to similar performances under balanced sinusoidal (ideal) supply conditions. However, the performance differs largely when the supply voltages are nonideal (distorted and/or unbalanced). The HF strategy obtains the HF source currents with compromised source power factor, while the UPF strategy achieves UPF at the expense of nonsinusoidal and unbalanced source currents.

It is well known that the power factor of the source currents can be improved by allowing similar harmonics into the source currents which are present into the supply voltages. However, the allowed harmonics into the source currents should not violate the current harmonic limits specified in IEEE Std. 519. Recently, several approaches have been proposed to combine the advantages of both HF and UPF control strategies using nonlinear optimization techniques [7]–[14]. The objective of the control techniques presented in [7]–[9] is to maximize the source power factor satisfying average power balance and source current total harmonic distortion (THD) constraints. As the constraints on individual harmonic distortion (IHD) are not considered in the problem formulation, the methods presented in [7]–[9] may not meet the IHD limits specified in IEEE Std. 519. On the other hand, the control techniques presented in [10]–[14] include the constraints on source current IHD along with THD and unbalance constraints in the problem formulation. Therefore, these methods can effectively meet the requirements of IEEE Std. 519 while maximizing the source power factor. However, such control approaches rely on the use of iterative techniques for solving the optimization problem. The iterative methods are difficult to implement digitally for the control of the shunt APF as the convergence time is dependent on the initial guess and operating point. In addition, there is a possibility of convergence failure and very high computational time which is often too high to be accommodated in one sampling period. This constrains the applicability of the aforementioned control approaches under dynamic load conditions. As a result, presumably, the methods discussed in [10]–[14] focused on steady-state load compensation only.

To overcome the issue of large computation time required to solve the optimization problem using iterative techniques, in this paper, a simple and straightforward method is proposed

Manuscript received November 24, 2013; revised February 11, 2014 and June 3, 2014; accepted June 27, 2014. Date of publication July 22, 2014; date of current version January 7, 2015. This work was supported by the Masdar Institute of Science and Technology under MISRG internal grant (Award 10PAAA2).

The authors are with the Masdar Institute of Science and Technology, Abu Dhabi, United Arab Emirates (e-mail: pkanjiya@masdar.ac.ae; vkhadkikar@masdar.ac.ae; hzaineldin@masdar.ac.ae).

Color versions of one or more of the figures in this paper are available online at http://ieeexplore.ieee.org.

Digital Object Identifier 10.1109/TIE.2014.2341559

to solve the shunt APF optimization problem noniteratively. The proposed algorithm is based on direct calculation of control variables without incorporating any iterative optimization technique. Therefore, it fulfills all of the requirements for its digital implementation and hence is promising for industrial application. The main contributions of this paper, compared to the previous work in [7]–[14], are listed as follows.

1) A noniterative solution to the optimization problem that includes constraints on individual harmonic limits is presented.
2) It achieves optimal power factor under any operating conditions satisfying IEEE Std. 519.
3) It is effective for dynamic load compensation.

The performance of the proposed noniterative algorithm is evaluated through a detailed experimental study. The experimental results highlight the effectiveness of the proposed algorithm, particularly under the load current and supply voltage dynamics.

II. Constrained Problem Formulation for Optimal Control of the Shunt APF

To achieve maximum power factor under distorted and unbalanced supply conditions, the source currents should have the same harmonic content and unbalance as the supply voltages. This suggests that, in case of highly distorted supply conditions, the source current THD, IHDs, and unbalance may not be within the acceptable limits specified in IEEE Std. 519. For the source current to meet the THD, IHD, and power balance constraints while maximizing the power factor, the APF control algorithm is formulated as an optimization problem. The control variables considered in the optimization problem are the conductance factor G_n for each individual harmonic order.

Let the desired source currents be expressed as follows:

$$i^*_{sx}(t) = \sum_{n=1}^{h} G_n v'_{sxn}(t), \quad x = a, b, c. \tag{1}$$

In (1), $*$ denotes the reference or desired quantity. G_n is the conductance factor for the nth order harmonic including fundamental, and $v'_{sxn}(t)$ is the balanced set of voltages extracted from distorted and unbalanced supply voltages. The balanced set of supply voltages can be obtained by either instantaneous symmetrical components as in [8] or multiple $d-q$ transformations as in [9]. It is worthy to note that the same conductance factors are used for each phase in (1) to obtain balanced source currents. As the desired source currents are balanced, the optimization problem is formulated considering only one phase.

A. Objective Function

The objective of the shunt APF control is to maximize the source power factor. This can be achieved by minimizing the apparent power supplied for a given active power requirement. Therefore, the objective function (f) to be minimized is selected as the square of the apparent power, which can be expressed as follows:

$$f = \sum_{n=1}^{h} V'^2_{sn} \sum_{n=1}^{h} G_n^2 V'^2_{sn} \tag{2}$$

where V'_{sn} is the rms value of the nth order balanced harmonic voltage.

B. Equality Constraint

To achieve balanced source currents, the total active power required by the load should be distributed equally in each phase. Therefore, the equality constraint can be written as

$$\frac{P_{\text{Lavg}} + P_{\text{Loss}}}{3} - \sum_{n=1}^{h} G_n V'^2_{sn} = 0 \tag{3}$$

where P_{Lavg} and P_{Loss} are the average load power and the shunt APF power loss, respectively.

C. Inequality Constraint

As discussed earlier, to meet the current harmonic limits specified in IEEE Std. 519, the upper limits on the source current THD and IHDs are considered as inequality constraints in the presented work. The upper bounds on source current THD and IHDs are denoted as $\text{THD}_{\max}$ and $\text{IHD}_{n\_\max}$, respectively. The inequality constraints on source current THD and IHDs are then given by

$$\frac{\sum_{n=2}^{h} G_n^2 V'^2_{sn}}{G_1^2 V'^2_{s1}} \le \text{THD}^2_{\max} \tag{4}$$

$$\frac{G_n^2 V'^2_{sn}}{G_1^2 V'^2_{s1}} \le \text{IHD}^2_{n\_\max}, \quad n = 2, 3, \ldots, h. \tag{5}$$

III. Proposed Noniterative Solution Incorporating Individual Current Harmonic Limits

The application of iterative optimization techniques to the real-time control of any system having fast dynamics might perform inadequately due to the following reasons.

1) The convergence time of the iterative optimization techniques is not fixed, and it varies with the following: a) different initial guesses and b) different operating points.
2) Under certain operating conditions, the iterative optimization techniques might fail to converge to the global minimum point.
3) Higher convergence time.

To resolve such problems, a noniterative approach is proposed. In [9], it is shown that the closed-form mathematical solution to the shunt APF optimization problem is possible if all of the constraints considered in the problem formulation are equality constraint. The inequality constraint on source current THD can be easily converted to equality constraint by comparing it to the source voltage THD [9]. However, the inequality

constraints on source current IHDs cannot be converted to equality constraints as the contribution of individual harmonics in source current decides the THD, and to fulfill the equality constraint on source current THD, IHDs should be allowed to take any value within their boundaries. Therefore, the shunt APF optimization problem is solved noniteratively in two parts. In the first part, the inequality constraints on IHDs given in (5) are excluded from the optimization problem, and the closed-form mathematical expressions for the optimal conductance factors are derived. In the second part, the mathematical expressions of optimal conductance factors derived in the first part are modified to handle the inequality constraints on IHDs without affecting the optimality of the solution.

A. Part 1: Problem Solution Excluding Constraints on IHDs

Let $\text{THD}_{\text{specified}}$ be the user-defined (prespecified) THD limit on the source current. As discussed earlier, the source power factor can be maximized by allowing similar amount of supply voltage harmonics into the source current. However, the THD in source current should not exceed $\text{THD}_{\text{specified}}$. This can be represented as

$$\left.\begin{aligned}\text{THD}_{\max} &= \text{THD}_{\text{specified}} && \text{if } \text{THD}_{\text{specified}} < \text{THD}_v\\ &= \text{THD}_v && \text{otherwise}\end{aligned}\right\} \quad (6)$$

where

$$\text{THD}_v = \frac{\sqrt{\sum_{n=2}^{h} V_{sn}'^2}}{V_{s1}'}. \quad (7)$$

With $\text{THD}_{\max}$ set as per (6) in the inequality constraint of (4), it will always reach its upper boundary to obtain maximal power factor. Therefore, the inequality constraint on source current THD can be rewritten as an equality constraint as follows:

$$\sum_{n=2}^{h} G_n^2 V_{sn}'^2 - \text{THD}_{\max}^2 G_1^2 V_{s1}'^2 = 0. \quad (8)$$

The optimization problem with the objective function of (2) and the equality constraint of (3) and (8) is a constrained nonlinear optimization problem where the control or decision variables are the conductance factors. Using the Lagrangian function, this problem can be transformed into an unconstrained optimization problem as follows [17]:

$$\mathcal{L} = \sum_{n=1}^{h} V_{sn}'^2 \sum_{n=1}^{h} G_n^2 V_{sn}'^2 + \lambda_1 \left(\frac{P_{\text{Lavg}} + P_{\text{Loss}}}{3} - \sum_{n=1}^{h} G_n V_{sn}'^2 \right) + \lambda_2 \left(\sum_{n=2}^{h} G_n^2 V_{sn}'^2 - \text{THD}_{\max}^2 G_1^2 V_{s1}'^2 \right). \quad (9)$$

By applying the Karush–Kuhn–Tucker (KKT) optimality conditions to (9) [17], the following set of equations can be derived:

$$\frac{\partial \mathcal{L}}{\partial G_1} = 2G_1 V_{s1}'^2 \sum_{n=1}^{h} V_{sn}'^2 - \lambda_1 V_{s1}'^2 - 2G_1 \lambda_2 V_{s1}'^2 \text{THD}_{\max}^2 = 0 \quad (10)$$

$$\frac{\partial \mathcal{L}}{\partial G_m} = 2G_m V_{sm}'^2 \sum_{n=1}^{h} V_{sn}'^2 - \lambda_1 V_{sm}'^2 - 2G_m \lambda_2 V_{sm}'^2 = 0, \quad m = 2, 3, \ldots, h \quad (11)$$

$$\frac{\partial \mathcal{L}}{\partial \lambda_1} = \frac{P_{\text{Lavg}} + P_{\text{Loss}}}{3} - \sum_{n=1}^{h} G_n V_{sn}'^2 = 0 \quad (12)$$

$$\frac{\partial \mathcal{L}}{\partial \lambda_2} = \sum_{n=2}^{h} G_n^2 V_{sn}'^2 - \text{THD}_{\max}^2 G_1^2 V_{s1}'^2 = 0. \quad (13)$$

From (11), it can be seen that the conductance factors for all harmonic orders will be equal and can be represented as follows:

$$G_2 = G_3 = \ldots\ldots\ldots\ldots = G_h = G_H. \quad (14)$$

By substituting (14) into (12) and (13), the following equations can be derived:

$$\frac{P_{\text{Lavg}} + P_{\text{Loss}}}{3} - V_{s1}'^2 \left(G_1 + G_H \text{THD}_v^2 \right) = 0 \quad (15)$$

$$\text{THD}_v^2 G_H^2 - \text{THD}_{\max}^2 G_1^2 = 0. \quad (16)$$

From (16), the normalized conductance factor for all harmonics G_{H_norm} can be represented as follows:

$$G_{H\_\text{norm}} = \frac{G_H}{G_1} = \frac{\text{THD}_{\max}}{\text{THD}_v}. \quad (17)$$

Furthermore, by substituting G_H from (17) into (15), an expression for G_1 can be derived as follows:

$$G_1 = \frac{P_{\text{Lavg}} + P_{\text{Loss}}}{3V_{s1}'^2 (1 + \text{THD}_{\max} \text{THD}_v)}. \quad (18)$$

B. Part 2: Dealing With Constraints on IHDs

It can be deduced from (14) in *part 1* that, if the inequality constraints on IHDs are excluded from the optimization problem, the conductance factors for all of the harmonic orders (excluding fundamental) turn out to be the same value as G_H. However, if the same conductance factor value is used for all of the harmonics, some harmonics may violate their IHD constraints. Therefore, it is necessary to update the value of the conductance factors for the harmonic orders whose IHD constraints are violated in order to satisfy their constraints. A step-by-step procedure has been developed to address this.

Let $\text{IHD}_n^{\text{specified}}$ be the user-defined IHD limit for the nth order harmonic.

Step 1) It is clear that, under the maximum power factor operation, the source current IHDs (IHD_{i_n}) should equate the source voltage IHDs (IHD_{v_n}). Therefore, if $\text{IHD}_n^{\text{specified}}$ is higher than IHD_{v_n}, to achieve maximum power factor, $\text{IHD}_{n\_\max}$ in (5) is set equal to IHD_{v_n}. On the other hand, if $\text{IHD}_n^{\text{specified}}$ is less than IHD_{v_n}, $\text{IHD}_{n\_\max}$ in (5) is set equal to $\text{IHD}_n^{\text{specified}}$ to assure that IHD_{i_n} is

below the limit. This can be mathematically represented as follows:

$$\left.\begin{aligned}\mathrm{IHD}_{n\_\max} &= \mathrm{IHD}_n^{\mathrm{specified}} && \text{if } \mathrm{IHD}_n^{\mathrm{specified}} < \mathrm{IHD}_{v_n}\\ &= \mathrm{IHD}_{v_n} && \text{otherwise}\end{aligned}\right\},$$
$$n = 2, 3, \ldots, h. \quad (19)$$

Step 2) The next step is to arrange the IHD constraints of different harmonic orders into descending order of their sensitivity to violate IHD limits. To achieve this, the constraint sensitivity factor (CSF) which is a measure of sensitivity to violate the IHD constraint is defined in (20). The index of the IHD constraints arranged into descending order with respect to their sensitivity to violate the IHD constraint is stored in a vector "y"

$$\mathrm{CSF}_n = \frac{\mathrm{IHD}_{v\_n}}{\mathrm{IHD}_n^{\mathrm{specified}}}. \quad (20)$$

Step 3) This step deals with satisfying IHD constraints of different harmonics in a sequential manner starting from the topmost sensitive (to violate the IHD constraint) harmonic. The IHD (IHD_{i_n}) of the most sensitive harmonic order (y (1): the first element of vector "y" is the index of the most sensitive harmonic) is first calculated using G_{H_norm} given in (17) as follows:

$$\mathrm{IHD}_{i\_y(1)} = \frac{G_H V'_{sy(1)}}{G_1 V'_{s1}} = G_{H\_\mathrm{norm}} \mathrm{IHD}_{v\_y(1)}. \quad (21)$$

Step 4) The calculated value of $\mathrm{IHD}_{i\_y(1)}$ as per (21) is then compared with its IHD limit $\mathrm{IHD}_{y(1)\_\max}$. If $\mathrm{IHD}_{i\_y(1)}$ is above this limit, then the normalized conductance factor for the harmonic under consideration $G_{\mathrm{norm}_{y(1)}}$ is calculated as per (22) by fixing its IHD limit else $G_{\mathrm{norm}\_y(1)}$ is updated with G_{H_norm}. The value of $G_{\mathrm{norm}\_y(1)}$ is then updated in the vector G_{norm}, which is a vector of normalized conductance factors

$$G_{\mathrm{norm}\_y(1)} = \frac{G_{y(1)}}{G_1} \begin{cases} = \dfrac{\mathrm{IHD}_{y(1)\_\max}}{\mathrm{IHD}_{v_{y(1)}}}, & \text{If } \mathrm{IHD}_{i_{y(1)}} > \mathrm{IHD}_{y(1)\_\max} \\ = G_{H\_\mathrm{norm}} & \text{else.} \end{cases} \quad (22)$$

If the IHD limit of the harmonic under consideration has been violated, then expressions for G_{H_norm} are updated as discussed in the following, or else, it will be kept the same as before.

The updated expression of G_{H_norm} can be derived by substituting $G_{y(1)}$ from (22) into the Lagrangian of (9) as

$$\begin{aligned}\mathcal{L} = &\sum_{n=1}^{h} V'^2_{sn} \left(G_1^2 V'^2_{s1} \left(1 + \mathrm{IHD}^2_{y(1)\_\max}\right) + \sum_{\substack{n=2 \\ n\neq y(1)}}^{h} G_n^2 V'^2_{sn} \right) \\ &+ \lambda_1 \left(\frac{P_{\mathrm{Lavg}} + P_{\mathrm{Loss}}}{3} \right. \\ &\quad - \left(G_1 V'^2_{s1} \left(1 + \mathrm{IHD}_{y(1)\_\max} \mathrm{IHD}_{v\_y(1)}\right) \right. \\ &\quad \left. \left. + \sum_{\substack{n=2 \\ n\neq y(1)}}^{h} G_n V'^2_{sn} \right) \right) \\ &+ \lambda_2 \left(\sum_{\substack{n=2 \\ n\neq y(1)}}^{h} G_n^2 V'^2_{sn} \right. \\ &\quad \left. - G_1^2 V'^2_{s1} \left(\mathrm{THD}^2_{\max} - \mathrm{IHD}^2_{y(1)\_\max} \right) \right). \end{aligned} \quad (23)$$

One can easily derive the updated expressions of G_{H_norm} and G_1 as (24) and (25), respectively, shown at the bottom of the page, by applying the KKT optimality condition to (23) and following the similar procedure given in *part 1*.

Using the updated expression of G_{H_norm}, the discussed procedure is repeated until all harmonic orders are addressed. There is no need to compute G_1 while dealing with IHD constraints; the updated expression for G_1 is just given for the reference of the readers. The generalized expressions to update G_{H_norm} and G_1 are given as (26) and (27), shown at the bottom of the next page.

In (26) and (27), "A" is a vector containing an index of harmonic order whose IHD constraints are active. Initially, vector "A" is an empty vector, and

$$G_{H\_\mathrm{norm}} = \frac{G_H}{G_1} = \sqrt{\frac{\mathrm{THD}^2_{\max} - \mathrm{IHD}^2_{y(1)\_\max}}{\mathrm{THD}^2_v - \mathrm{IHD}^2_{v\_y(1)}}} \quad (24)$$

$$G_1 = \frac{P_{\mathrm{Lavg}} + P_{\mathrm{Loss}}}{3V'^2_{s1}\left(1 + \mathrm{IHD}_{y(1)\_\max}\mathrm{IHD}_{v_{y(1)}} + \sqrt{\left(\mathrm{THD}^2_{\max} - \mathrm{IHD}^2_{y(1)\_\max}\right)\left(\mathrm{THD}^2_v - \mathrm{IHD}^2_{v_{y(1)}}\right)}\right)} \quad (25)$$

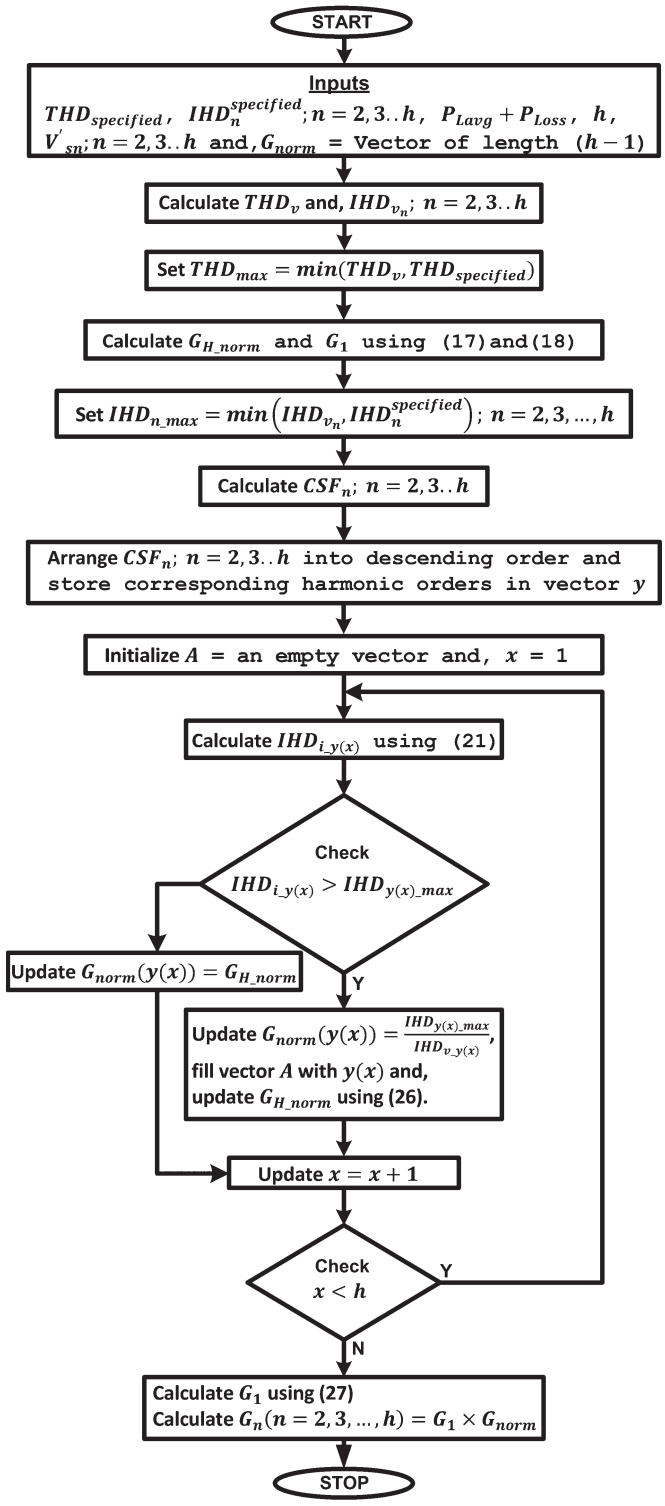

Fig. 1. Flowchart of the proposed noniterative approach.

TABLE I
DIFFERENT TEST CASES FOR ROBUSTNESS ANALYSIS

Operating condition	V'_{s1}	V'_{s2}	V'_{s3}	V'_{s4}	V'_{s5}	V'_{s6}	V'_{s7}	P_{Tavg}
Case-1	1	0.02	0.03	0.02	0.05	0.02	0.05	1
Case-2	1	0.00	0.00	0.02	0.05	0.00	0.00	1
Case-3	1	0.02	0.03	0.02	0.05	0.02	0.05	0.3
Case-4	1	0.0	0.00	0.02	0.05	0.00	0.00	0.5

it is filled with the index of active IHD constraints during the aforementioned process of dealing with IHD constraints.

Step 5) Finally, the optimal fundamental conductance factor G_1 is calculated using (27), and it is multiplied to vector G_{norm} to obtain the optimal conductance factors for harmonics.

A flowchart of the proposed noniterative approach to compute the optimal conductance factors is given in Fig. 1.

IV. ROBUSTNESS ANALYSIS

The proposed noniterative method has been applied to solve the optimization problem formulated in Section II at different operating points. The accuracy of the proposed method to achieve optimal results is proven by comparing its results with those achieved using the Newton–Raphson (NR) optimization technique. The different test cases for which the optimization problem has been solved are given in Table I. It is assumed that the highest order harmonic present in the supply voltages is seventh. The steady state per unit values (rms) of the extracted fundamental and harmonic voltages with total per unit powers $[P_{\text{Tavg}}(P_{\text{Lavg}} + P_{\text{Loss}})]$ for different test cases are tabulated in Table I. The upper bound on source current THD is specified as 5%, while the IHD limits for individual odd and even harmonics are specified as 4% and 1%, respectively, as per IEEE Std. 519.

The CPU used for this study has core i5 processor with a 4-GB RAM. For the NR method, the optimization problem with seven conductance factors is formulated and solved using MATLAB optimization tool box, while for the proposed method, the code is written in MATLAB (m-file). The results achieved with both methods for different test cases are tabulated in Table II. To show the dependence of the NR method on the initial guess, two different initial guesses for the conductance factor are considered: 1) The initial values of all of the conductance factors are set to zero (NR-0), and 2) the initial values of all of the conductance factors are set to one (NR-1). From the results provided in Table II, it can be seen that, for *case 1* and

$$G_{H\_\text{norm}} = \frac{G_H}{G_1} = \sqrt{\frac{\text{THD}_{\max}^2 - \sum_{n\in A} \text{IHD}_{n\_\max}^2}{\text{THD}_v^2 - \sum_{n\in A} \text{IHD}_{v\_n}^2}} \tag{26}$$

$$G_1 = \frac{P_{\text{Lavg}} + P_{\text{Loss}}}{3V_{s1}'^2\left(1 + \sum_{n\in A} \text{IHD}_{n\_\max}\text{IHD}_{v\_n} + \sqrt{\left(\text{THD}_{\max}^2 - \sum_{n\in A} \text{IHD}_{n\_\max}^2\right) * \left(\text{THD}_v^2 - \sum_{n\in A} \text{IHD}_{v\_n}^2\right)}\right)} \tag{27}$$

TABLE II
COMPARISON OF DIFFERENT METHODS TO SOLVE AN OPTIMIZATION PROBLEM

Parameters	Case-1			Case-2			Case-3			Case-4		
	NR-0	NR-1	PR	NR-0	NR-1	PR	NR-0	NR-1	PR	NR-0	NR-1	PR
Fcn. Value	0.1112	0.1112	0.1112	0.1111	0.1111	0.1111	0.0101	0.0100	0.0100	0.0279	0.0278	0.0278
G_1	0.3319	0.3319	0.3319	0.3326	0.3326	0.3326	0.1000	0.0996	0.0996	0.1667	0.1663	0.1663
G_2	0.1660	0.1660	0.1660	-	-	-	0.0000	0.0498	0.0498	-	-	-
G_3	0.2027	0.2027	0.2027	-	-	-	0.0001	0.0608	0.0608	-	-	-
G_4	0.1660	0.1660	0.1660	0.1663	0.1663	0.1663	0.0000	0.0498	0.0498	0.0001	0.0832	0.0832
G_5	0.2027	0.2027	0.2027	0.2661	0.2661	0.2661	0.0002	0.0608	0.0608	0.0004	0.1330	0.1330
G_6	0.1660	0.1660	0.1660	-	-	-	0.0000	0.0498	0.0498	-	-	-
G_7	0.2027	0.2027	0.2027	-	-	-	0.0002	0.0608	0.0608	-	-	-
P_{calc} (pu)	1	1	1	1	1	1	0.3	0.3	0.3	0.5	0.5	0.5
THD_{calc}(%)	5	5	5	4.12	4.12	4.12	0.0179	5	5	0.0125	4.12	4.12
IHD_{2_calc}(%)	1	1	1	0	0	0	0.0008	1	1	0	0	0
IHD_{3_calc}(%)	1.83	1.83	1.83	0	0	0	0.0027	1.83	1.83	0	0	0
IHD_{4_calc}(%)	1	1	1	1	1	1	0.0008	1	1	0.0008	1	1
IHD_{5_calc}(%)	3.05	3.05	3.05	4	4	4	0.0125	3.05	3.05	0.0125	4	4
IHD_{6_calc}(%)	1	1	1	0	0	0	0.0008	1	1	0	0	0
IHD_{7_calc}(%)	3.05	3.05	3.05	0	0	0	0.0125	3.05	3.05	0	0	0
Time(μ-sec)	30000	37000	**35**	25925	31958	**34**	18133	35300	**35**	17900	20364	**35**

case 2, the results achieved with the NR-0, NR-1, and proposed (PR) methods are identical. However, the times required by the NR-0 and NR-1 methods to reach the optimal solution are 30 and 37 ms, respectively, which are quite high compared to the 35-μs time required by the proposed method. In addition, due to the different initial guesses, the time required by the NR-0 and NR-1 methods is different. It can be noticed from the results of *case 3* and *case 4* that the NR-0 method fails to converge at the global minimum and it is trapped in a local minimum, while the NR-1 and proposed methods are able to find the global minimum. Moreover, by comparing the times required by the different methods for different operating conditions, it can be deduced that the times required by the NR methods (both NR-0 and NR-1) with different operating points differ as opposed to almost a constant time for the proposed method.

From the aforementioned case study, it can be concluded that the proposed approach is very robust to changes in operating conditions as opposed to the NR method. The distinguishing features of the proposed noniterative optimized approach, which makes it favorable for the control of the shunt APF for steady state as well as dynamic load compensation, can be summarized as follows:

1) very low and almost constant computation time;
2) guaranteed convergence;
3) independence on the initial guess.

V. OVERALL CONTROL BLOCK OF THE SHUNT APF

Fig. 2 presents the system under study, which consists of an equivalent grid behind an impedance, the combined linear and nonlinear three-phase loads, and the shunt APF. The four-leg voltage source inverter (VSI) topology is utilized to realize the 3P4W APF system.

The overall control block diagram of the proposed single-step noniterative optimized control algorithm is shown in Fig. 3. The inputs to the calculation of the optimized

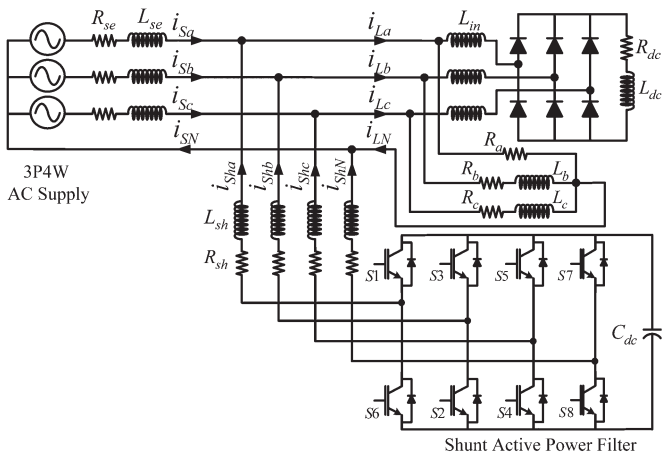

Fig. 2. Four-leg VSI-based shunt APF system configuration.

conductance factor block are the specified source current THD limit ($\text{THD}_{\text{specified}}$), IHD limits for different harmonics ($\text{IHD}_n^{\text{specified}}$), demanded average total power ($P_{\text{Lavg}} + P_{\text{Loss}}$), and rms values of the balanced set of harmonic voltages ($V'sn'\ n = 1, 2 \ldots, h$). The instantaneous load power is calculated as

$$P_L(t) = v_{sa} i_{La} + v_{sb} i_{Lb} + v_{sc} i_{Lc}. \tag{28}$$

The instantaneous power $P_L(t)$ is then processed by a moving average filter (MAF) to obtain the average power P_{Lavg}. To maintain the dc link capacitor voltage constant at a prespecified value, a small amount of active power (P_{Loss}) should be drawn from the grid. To accomplish this, a proportional–integral (PI) controller is used to control the average dc link voltage. After calculating the conductance factors G_n for all of the harmonic orders including fundamental, as shown in Fig. 3, the three-phase reference source currents are calculated as in (1). When harmonics, multiple of three, are present in the reference source currents, they should flow through the source neutral conductor. Therefore, the reference source neutral current is set equal to

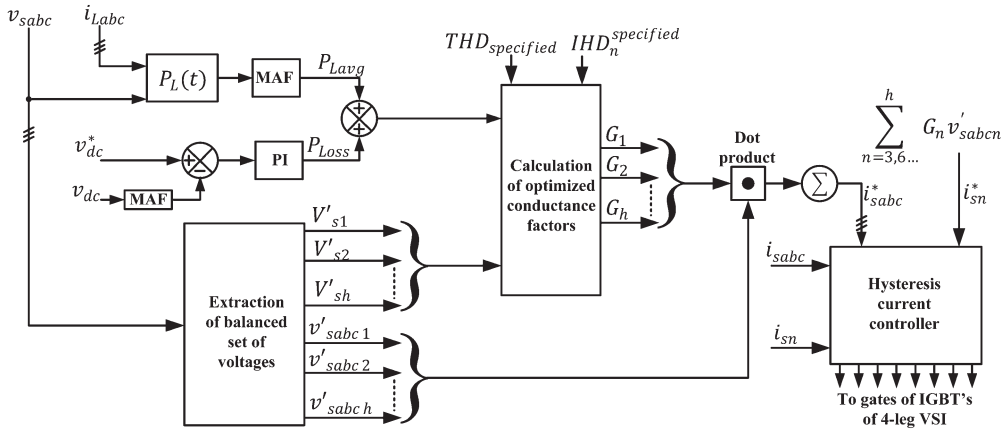

Fig. 3. Overall control block diagram of the proposed noniterative optimized control of the four-leg VSI-based shunt APF.

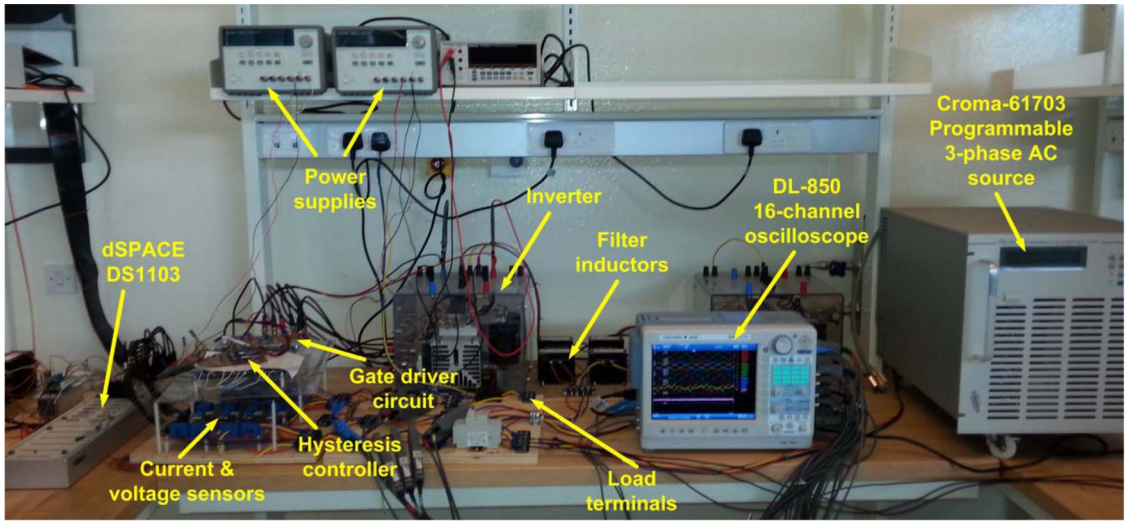

Fig. 4. Laboratory prototype of the shunt APF.

the sum of all of the triplen harmonics of all phases. These reference source currents are then compared with the actual measured currents using the hysteresis current controller which determines the switching signals for the VSI.

VI. Experimental Validation

The proposed noniterative optimized approach is validated by conducting a detailed experimental study on a shunt APF laboratory prototype shown in Fig. 4. The experimental test system data are given in the Appendix. The Croma-61703 programmable three-phase ac source is used to generate nonideal supply voltages. The seven signals necessary to implement the proposed control algorithm (the three supply voltages, the three load currents, and the dc bus voltage) are sensed using Hall effect current and voltage transducers. The reference source currents are generated by implementing the proposed control algorithm (Fig. 3) into the dSPACE-1103 digital signal processor (DSP) board with 40-μs sampling time. These generated reference source currents (total of four: three for phase currents and one for neutral) are taken out of the DSP through DAC ports. An external analog hysteresis current control board is developed to perform the pulsewidth modulation. The actual and reference source current signals are compared using analog hysteresis board to generate the switching pulses for the shunt inverter. For the experimental studies, the maximum order of harmonic present into the supply voltages is considered to be seven. The nonideal supply voltages considered for the experimental studies are given in Table III.

TABLE III
Distorted and Unbalanced Supply Voltages

Phase-a	*Phase-b*	*Phase-c*
$70.71\sin(\omega t)$	$84.85\sin(\omega t-110)$	$56.57\sin(\omega t+90)$
$+4.24\sin(2\omega t)$	$+5.09\sin(2(\omega t-110))$	$+3.39\sin(2(\omega t+90))$
$+2.83\sin(4\omega t)$	$+3.39\sin(4(\omega t-110))$	$+2.26\sin(4(\omega t+90))$
$+7.07\sin(5\omega t)$	$+8.49\sin(5(\omega t-110))$	$+5.66\sin(5(\omega t+90))$
$+3.54\sin(7\omega t)$	$+4.24\sin(7(\omega t-110))$	$+2.83\sin(7(\omega t+90))$

The performance of the shunt APF is evaluated for steady-state load condition as well as under load variations and supply voltage variations. The measured values of the THD and IHDs of the supply voltages as well as load currents up to the seventh-order harmonic along with load power factor (PF) are tabulated in Table IV.

TABLE IV
DIFFERENT INDICES OF SUPPLY VOLTAGES AND LOAD CURRENTS

Quantity	*THD*	*IHD(%)*						*Load*
	(%)	*2nd*	*3rd*	*4th*	*5th*	*6th*	*7th*	*PF*
a	13.3	06.0	0.20	04.1	10.1	0.05	05.0	
Voltage-b	13.2	06.0	0.10	04.0	10.0	0.02	05.0	-
c	13.0	06.0	0.06	04.0	10.0	0.03	05.0	
a	17.3	10.0	07.4	04.5	05.4	05.3	03.7	0.981
Current-b	15.0	06.8	06.0	05.6	05.5	03.6	05.0	0.834
c	23.5	06.5	06.9	04.9	16.2	02.9	09.4	0.931

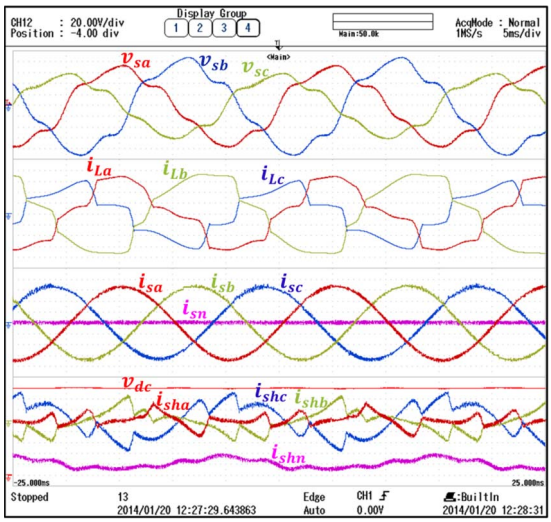

Fig. 5. Steady-state experimental results (mode 1).

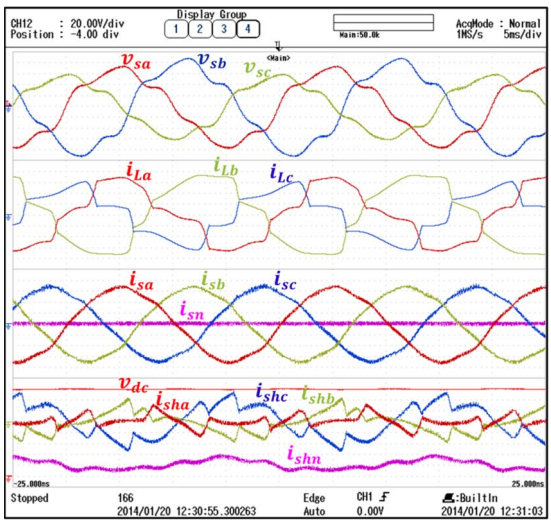

Fig. 6. Steady-state experimental results (mode 2).

A. Performance Evaluation Under Steady-State Load Condition

To show the flexibility and superiority of the proposed control algorithm over conventional approaches, three different control modes of operation for the shunt APF are considered, which are as follows: $\text{THD}_{\text{specified}} = 0\%$ with open IHD limits (HF strategy), $\text{THD}_{\text{specified}} = 5\%$ with open IHD limits, and $\text{THD}_{\text{specified}} = 5\%$ with $\text{IHD}_n^{\text{specified}} = 4\%$ for individual odd harmonics and $\text{IHD}_n^{\text{specified}} = 1\%$ for individual even harmonics as per IEEE Std. 519.

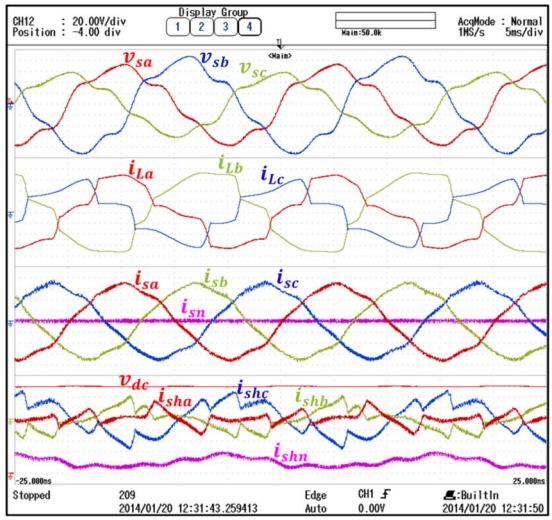

Fig. 7. Steady-state experimental results (mode 3).

TABLE V
DIFFERENT PERFORMANCE INDICES ACHIEVED USING THE SHUNT APF

Mode	*THD*	*IHD(%)*				*Source PF*		
	(%)	*2nd*	*4th*	*5th*	*7th*	*a*	*b*	*c*
mode-1	1.4	0.1	0.2	0.7	0.2	0.986	0.956	0.891
mode-2	5.1	**3.5**	**1.4**	2.7	2.1	0.992	0.962	0.893
mode-3	5.2	1.0	1.0	4.0	2.8	0.992	0.963	0.893

The experimental results with the proposed optimized algorithm for the aforementioned three modes of operation are given in Figs. 5–7. A 16-channel oscilloscope (Yokogawa DL850) was used to capture the experimental results. The oscilloscope display format was set to four groups, dividing the screen into four parts. The nonideal supply voltages (v_{sa}, v_{sb}, v_{sc}) and the nonlinear load currents (i_{La}, i_{Lb}, i_{LC}) are displayed in the first and second groups, respectively. The source currents (i_{sa}, i_{sb}, i_{sc}) along with the source neutral current (i_{sn}) are depicted in the third group, while the compensating currents $(i_{sha}, i_{shb}, i_{shc}, i_{shn})$ and the dc link voltage (v_{dc}) are displayed in the fourth group. All of the voltage signals are measured with the scale of 20 V/division, while all of the current signals are measured with 1 A/division. The phase-a source current THD and IHDs (as all three-phase currents are identical) are also measured and tabulated in Table V, along with three-phase source power factors. It can be noticed from Fig. 5 that, for the HF mode of operation (mode 1), the source currents are achieved as balanced and sinusoidal. In this mode of operation, the THD of the source current is 1.4%.

The profile of the source currents when the shunt APF operates in mode 2 is given in Fig. 6. It can be seen that the source currents are slightly distorted with the similar harmonics present in the supply voltages to maximize the power factor. The improvement in the power factor compared to mode 1 can be noticed from Table V. In this mode of operation, the THD of the source current is 5.1% (slightly higher than $\text{THD}_{\text{specified}}$ due to the switching harmonics). As the IHD constraints are not imposed in this mode, the second and fourth harmonics in the source currents are measured as 3.5% and 1.4%, respectively (shown in bold and shaded in Table V), which are above the individual even harmonic limit of 1% recommended by IEEE Std. 519.

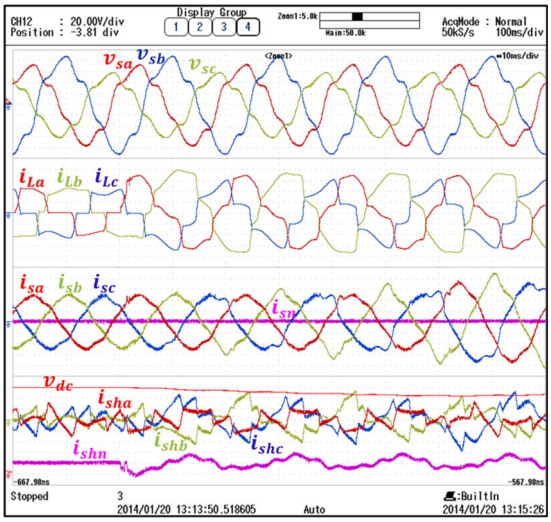

Fig. 8. Experimental results during load dynamics (NR method).

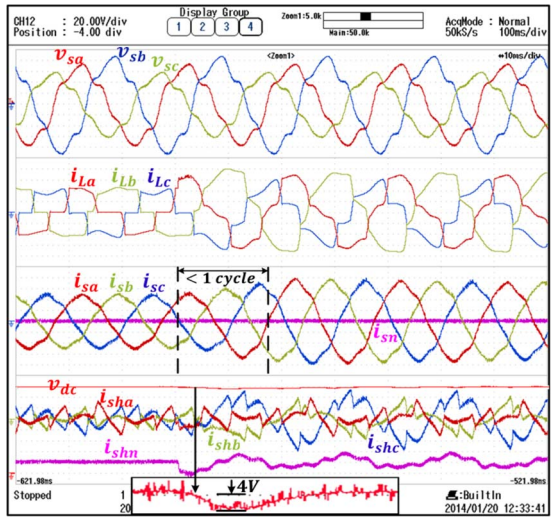

Fig. 9. Experimental results during load dynamics (proposed method).

Finally, the performance of the shunt APF under mode 3 is evaluated, where both THD and IHD constraints are made active. The profile of the source currents with this mode of operation is depicted in Fig. 7. It should be noticed that the source currents are slightly different from those of mode 2 (Fig. 6) as the amount of individual harmonics in the source currents is different in both modes. Due to imposition of the IHD constraints, the second and fourth harmonics are limited to 1% (Table V). In addition, the odd harmonics (fifth and seventh) in the source currents, for both modes 2 and 3, are found within the individual odd harmonic limit as per IEEE Std. 519. The source current power factors and THD achieved in this mode are almost identical to that of mode 2.

It can be observed from the previously discussed three modes of operation that the source current power factor, in the optimized mode, is better than HF operation. Moreover, the proposed approach with both THD and IHD constraints is able to satisfy IEEE Std. 519. It is evident from the experimental results that, in all of the aforementioned operating modes, the fourth leg of the shunt APF effectively compensates the load neutral current and makes the neutral current flowing through the source (i_{sn}) equal to zero.

B. Performance Evaluation Under Dynamic Load Condition

One of the significant features of the proposed algorithm is low computation time (less than 40 μs for the overall algorithm) which is due to the use of a noniterative approach for solving the optimization problem. This makes the proposed algorithm superior over iterative optimization techniques when applied for dynamic load compensation [10]–[14]. To highlight this, a comparative study under dynamic load conditions is performed and verified experimentally. For the implementation of an iterative-method-based APF control, the optimized conductance factors in Fig. 3 are calculated using the NR method. It is found that the NR method requires a sampling time of 40 ms to calculate the optimized conductance factors. Therefore, it is implemented in an outer control loop with 40-ms sampling time, while other control tasks are implemented with 40-μs sampling time in an inner control loop. The performance of the NR method during a sudden load change condition is illustrated in Fig. 8. The dynamic condition is created by changing the load from $L1$ to $L1 + L2$ (Appendix). It can be observed from the initial few cycles that, even after the load change, the NR-method-based controller compensates the source currents based on the previously computed conductance factors (for load condition $L1$). This is due to the large computation time required by the NR method. As the active power required by the new load $(L1 + L2)$ is higher than load $L1$, the dc link voltage drops to a value where APF loses its compensation capability and, thus, its control over the source currents.

Under the same dynamic condition, the performance of the proposed control algorithm is given in Fig. 9. As noticed, the APF system with the proposed noniterative optimized approach achieves the new steady-state condition within one cycle (time taken by the source currents to adapt to the new loading condition) without affecting the APF compensation capability during load change. Furthermore, the dc link controller effectively regulates the dc bus voltage at the set reference value (see zoomed window at the bottom of Fig. 9). The three-phase source current THDs obtained by the proposed and NR methods under the new operating condition are compared in Table VI. It can be noticed that the proposed method is able to control the source current THDs to the desired level, while the NR method fails to control them due to the reduction in dc link voltage. The ability of compensating dynamic load demonstrates the capability and enhanced performance of the proposed noniterative optimized algorithm over other optimization-based approaches.

C. Performance Evaluation Under Supply Voltage Dynamics

It is important to study the performance of the shunt APF under supply voltage dynamics as the source currents are a function of the supply voltages. The performance of the proposed control algorithm during a sudden change in supply voltages is illustrated in Fig. 10. Initially, the supply voltages were

TABLE VI
SOURCE CURRENT THD COMPARISON BETWEEN THE PROPOSED AND NR METHODS (BEFORE AND AFTER COMPENSATION)

Phase	% Source current THD (Before compensation)	% Source current THD (After compensation)	
		Proposed	NR
a	17.3	5.18	6.72
b	15.0	5.16	13.43
c	23.5	5.19	15.41

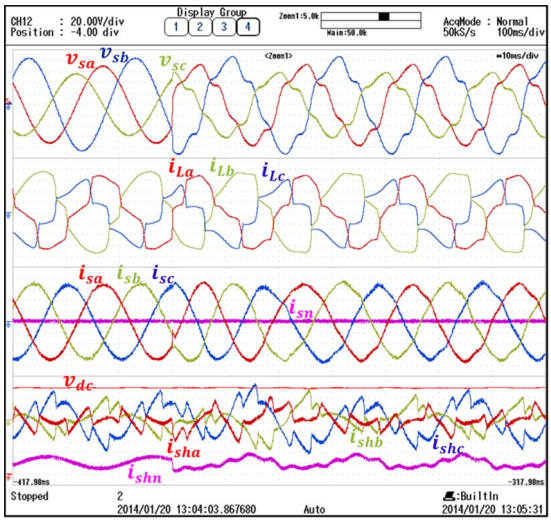

Fig. 10. Experimental results during supply dynamics (mode 3).

considered to have only fundamental voltages given in Table II. Suddenly, the harmonic voltages specified in Table II are added to the fundamental voltages. Furthermore, an arbitrary phase jump is given to these nonideal voltages to create this dynamic condition. The change in supply voltage profile is depicted in Fig. 10. It can be seen that the source currents become distorted to maximize the power factor within one cycle from the change in supply voltage. The one cycle delay in compensation is due to the delay caused by the extraction of the balanced set of voltages because of the MAFs. Also, note that the dc link voltage does not experience any change during this dynamic condition.

The compensation capability and adaptability of the proposed noniterative optimization method can be noted from Fig. 10. The source currents, before dynamic condition, are sinusoidal due to the sinusoidal source voltage. After dynamic voltage change, as the source voltage becomes distorted, the proposed approach determines the new reference currents (which maximize the power factor while satisfying IEEE Std. 519) within one cycle. During this operation, the source voltage and source current THDs are 0.5% and 1.4% (sinusoidal voltage condition), and 13.3% and 5.1% (distorted voltage condition), respectively.

VII. CONCLUSION

In this paper, a noniterative optimized control algorithm has been proposed for the shunt APF to achieve the maximum power factor satisfying power balance and current harmonic constraints as per IEEE Std. 519. The constraints on current harmonics include limits on the individual odd harmonics (set at 4%) and individual even harmonics (set at 1%) with THD not exceeding 5%. The robustness analysis of the proposed noniterative approach, carried out with different operating conditions and compared with the NR method, demonstrates that it always converges to an optimal solution. Furthermore, the time required by the proposed control algorithm is 35 μs, which is far lower than the NR method (between 20.364 and 35.3 ms). Finally, the proposed control algorithm is validated experimentally under steady-state as well as different dynamic conditions. The dynamic results exhibit the superiority of the proposed control algorithm, where it achieves the new operating condition within one to two cycles.

APPENDIX

The system data for the experimental study are given in the following:

APF	DC link capacitor = 2200 µF; reference DC link voltage = 160 V; filter inductor = 5mH DSP sampling time = 40 µ-sec Time period of MAF = 0.02 sec (one cycle)
Loads	L1 : 3-phase diode rectifier with 2.5mH input inductance: DC load- R=58Ω, L=100mH L2 :- phase-a: R=58Ω, L=0mH phase-b: R=29Ω, L=100mH phase-c: R=29Ω, L=100mH

REFERENCES

[1] B. Singh, K. Al-Haddad, and A. Chandra, "A review of active filters for power quality improvement," *IEEE Trans. Ind. Electron.*, vol. 46, no. 5, pp. 960–971, Oct. 1999.
[2] M. I. M. Montero, E. R. Cadaval, and F. B. Gonzalez, "Comparison of control strategies for shunt active power filters in three-phase four-wire systems," *IEEE Trans. Power Electron.*, vol. 22, no. 1, pp. 229–236, Jan. 2007.
[3] Q.-N. Trinh and H.-H. Lee, "An advanced current control strategy for three-phase shunt active power filters," *IEEE Trans. Ind. Electron.*, vol. 60, no. 12, pp. 5400–5410, Dec. 2013.
[4] M. Hamad, M. Masoud, K. Ahmed, and B. W. Williams, "A shunt active power filter for a medium-voltage twelve-pulse current source converter using open loop control compensation," *IEEE Trans. Ind. Electron.*, vol. 61, no. 11, pp. 5840–5850, Nov. 2014.
[5] M. Angulo, J. Lago, D. Ruiz-Caballero, S. Mussa, and M. Heldwein, "Active power filter control strategy with implicit closed loop current control and resonant controller," *IEEE Trans. Ind. Electron.*, vol. 60, no. 7, pp. 2721–2730, Jul. 2013.
[6] M. Qasim, P. Kanjiya, and V. Khadkikar, "Artificial neural network based phase locking scheme for active power filters," *IEEE Trans. Ind. Electron.*, vol. 61, no. 8, pp. 3857–3866, Aug. 2014.
[7] S. George and V. Agarwal, "A DSP based optimal algorithm for shunt active filter under nonsinusoidal supply and unbalanced load conditions," *IEEE Trans. Power Electron.*, vol. 22, no. 2, pp. 593–601, Mar. 2007.
[8] K. R. Uyyuru, M. K. Mishra, and A. Ghosh, "An optimization-based algorithm for shunt active filter under distorted supply voltages," *IEEE Trans. Power Electron.*, vol. 24, no. 5, pp. 1223–1232, May 2009.
[9] P. Kanjiya, V. Khadkikar, and H. Zeineldin, "A noniterative optimized algorithm for shunt active power filter under distorted and unbalanced supply voltages," *IEEE Trans. Ind. Electron.*, vol. 60, no. 12, pp. 5376–5390, Dec. 2013.
[10] S. M.-R. Rafiei, H. A. Toliyat, R. Ghazi, and T. Gopalarathnam, "An optimal and flexible control strategy for active filtering and power factor correction under non-sinusoidal line voltages," *IEEE Trans. Power Del.*, vol. 16, no. 2, pp. 297–305, Apr. 2001.

[11] G. W. Chang and C. M. Yeh, "Optimisation-based strategy for shunt active power filter control under non-ideal supply voltages," *Proc. Inst. Elect. Eng.—Elect. Power Appl.*, vol. 152, no. 2, pp. 182–190, Mar. 4, 2005.
[12] G. W. Chang, C.-M. Yeh, and W.-C. Chen, "Meeting IEEE-519 current harmonics and power factor constraints with a three-phase three-wire active power filter under distorted source voltages," *IEEE Trans. Power Del.*, vol. 21, no. 3, pp. 1648–1654, Jul. 2006.
[13] G. W. Chang, "A new approach for optimal shunt active power filter control considering alternative performance indices," *IEEE Trans. Power Del.*, vol. 21, no. 1, pp. 406–413, Jan. 2006.
[14] S. George and V. Agarwal, "Optimum control of selective and total harmonic distortion in current and voltage under nonsinusoidal conditions," *IEEE Trans. Power Del.*, vol. 23, no. 2, pp. 937–944, Apr. 2008.
[15] *IEEE Recommended Practices and Requirements for Harmonic Control in Electrical Power Systems*, IEEE Std. 519–1992, 1993.
[16] *IEEE Standard Definitions for the Measurement of Electric Power Quantities Under Sinusoidal, Nonsinusoidal, Balanced, or Unbalanced Conditions*, IEEE Std. 1459–2010, Mar. 19, 2010 (Revision of IEEE Standard 1459-2000).
[17] A. J. Wood and B. Wollenberg, *Power Generation Operation and Control*., 2nd ed. Hoboken, NJ, USA: Wiley Interscience, 1996.
[18] W. Forst and D. Hoffmann, *Optimization—Theory and Practice*. New York, NY, USA: Springer-Verlag, 2010.

Parag Kanjiya received the Bachelor's degree in engineering (electrical) from B.V.M. Engineering College, Sardar Patel University, V.V. Nagar, India, in 2009 and the Master's degree in technology (power systems) from the Indian Institute of Technology Delhi (IITD), New Delhi, India, in 2011.

Since October 2011, he has been a Research Engineer with the Masdar Institute of Science and Technology, Abu Dhabi, United Arab Emirates. His research interests include applications of power electronics in distribution systems, power quality enhancement, renewable energy, FACTS devices, and power system optimization.

Mr. Kanjiya was a recipient of the K.S. Prakasa Rao Memorial Award for getting the highest C.G.P.A at IITD in August 2011.

Vinod Khadkikar (S'06–M'09) received the B.E. degree in electrical engineering from the Government College of Engineering, Dr. Babasaheb Ambedkar Marathwada University, Aurangabad, India, in 2000, the M.Tech. degree in electrical engineering from the Indian Institute of Technology (IITD), New Delhi, India, in 2002, and the Ph.D. degree in electrical engineering from the École de Technologie Supérieure (E.T.S.), Montréal, QC, Canada, in 2008.

From December 2008 to March 2010, he was a Postdoctoral Fellow with the University of Western Ontario, London, ON, Canada. From April 2010 to December 2010, he was a Visiting Faculty with Massachusetts Institute of Technology, Cambridge, MA, USA. He is currently an Associate Professor with the Masdar Institute of Science and Technology, Abu Dhabi, United Arab Emirates. He is currently an Associate Editor of the *IET Power Electronics* journal. His research interests include applications of power electronics in distribution systems and renewable energy resources, grid interconnection issues, power quality enhancement, active power filters, and electric vehicles.

Hatem H. Zeineldin (M'06–SM'13) received the B.Sc. and M.Sc. degrees in electrical engineering from Cairo University, Cairo, Egypt, in 1999 and 2002, respectively, and the Ph.D. degree in electrical and computer engineering from the University of Waterloo, Waterloo, ON, Canada, in 2006.

He was with Smith and Andersen Electrical Engineering, Inc., where he was involved with projects involving distribution system design, protection, and distributed generation. He was then a Visiting Professor with Massachusetts Institute of Technology, Cambridge, MA, USA. He was with the Faculty of Engineering, Cairo University. He is currently an Associate Professor with the Masdar Institute of Science and Technology, Abu Dhabi, United Arab Emirates. His current interests include power system protection, distributed generation, and microgrids.

Dr. Zeineldin is currently an Editor of the IEEE TRANSACTIONS ON ENERGY CONVERSION.